VIBRATION PARAMETER ESTIMATION USING FMCW RADAR

*Lei Ding**, *Murtaza Ali**, *Sujeet Patole*† *and Anand Dabak**

*Texas Instruments, Dallas, Texas †University of Texas at Dallas, Richardson, Texas

ABSTRACT

Vibration sensing is essential in many applications. Traditional vibration sensors are contact based. With the advance of low-cost and highly integrated CMOS radars, another class of non-contact vibration sensors is emerging. In this paper, we present detailed analysis on obtaining vibration parameters using frequency modulated continuous wave (FMCW) radars. We establish the Cramer Rao lower bounds (CRLB) of the parameter estimation problem and propose an estimation algorithm that achieves the bounds in simulations. These analysis show that vibration sensing using FMCW radars can easily achieve sub-Hertz frequency accuracy and micrometer level amplitude accuracy.

Index Terms— frequency modulated continuous wave (FMCW) radars, vibration sensors, Cramer Rao lower bound, parameter estimation.

1. INTRODUCTION

Vibration monitoring and analysis is an important tool in many applications. In rotary machinery [1], such as motors and engines, it can help to achieve optimum performance and provide early indications of faulty components. In structure health monitoring [2], it can be used to monitor the health of bridges and buildings to ensure the safety of these structures. In health care, the movement of human chests is also a vibration signal that provides information about respiration and heart rates [3].

Traditionally, most vibration monitoring applications use contact-based vibration sensors, such as accelerometers. With the development of low cost and highly integrated CMOS radars [4, 5], another class of vibration sensors is emerging, which allows non-contact measurements of vibration signals. The non-contact approach is more flexible and avoids any coupling issues between sensors and vibration objects.

Among different architectures for radar based vibration sensors, the frequency-modulated continuous wave (FMCW) [6] architecture is one of the most flexbile. In a FMCW system (see Fig. 1), a periodic chirp signal is generated by a frequency synthesizer and transmitted to the target. The mixing of reflected signal and the transmitted signal results in a low frequency beat signal, whose frequency directly corresponds to the range of the target. The phase of the beat signal across multiple chirps can be tracked to provide vibration or Doppler information of the target. The architecture is also well-suited for low-cost CMOS implementation due to the low peak-to-average power ratio of the transmitted signal, which allows higher efficiency power amplifier operation. Because of these advantages, we focus on vibration parameter estimation using the FMCW approach in this paper. In Section 3, we present the details of FMCW radar signal processing. New Cramer-Rao lower bounds (CRLB) for vibration parameter estimates are derived in Section 4. We then set up simulations and present a new estimation algorithm that achieves the bounds in Section 5. Finally, we conclude in Section 6.

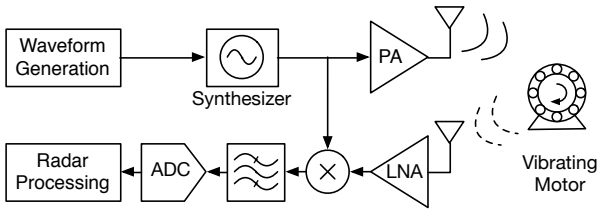

Fig. 1. Simplified block diagram of a FMCW radar system.

2. RELATION TO PRIOR WORK

Vibration signal extraction using FMCW radar has been presented in [7] in the context of human vital sign detection. But no performance bounds are available to understand the theoretical limits of the estimation approach. Previous CRLB bounds derived for single tone parameter estimation [6] and motion parameter estimation for dual-frequency radar [8] cannot be applied here because of different signal models. The main contribution of this paper is the new CRLBs for these type of estimation problems and a new algorithm that achieves the performance bounds in simulations.

3. FMCW RADAR SIGNAL PROCESSING

Fig. 2 shows typical transmitted and received chirp signals in an FMCW system. Denoting the time within each chirp ramp period as t, i.e., $0 < t < T_r$, a single transmitted chirp signal is defined as

$$s(t) \quad = \quad \exp\left[j(2\pi f_c t + \pi K t^2)\right],\ K = \frac{B}{T_r}, \qquad (1)$$

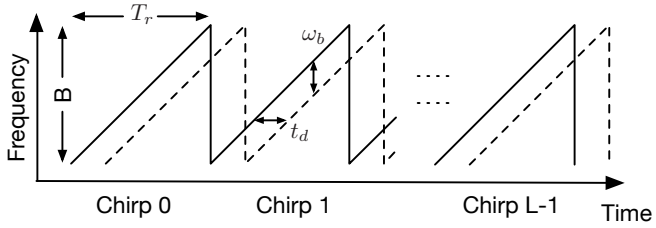

Fig. 2. A sequency of L transmitted (solid line) and received (dashed line) chirp signals.

where f_c is the carrier frequency, and B is the bandwidth of the chirp signal. Assume that the distance between the target and the radar is

$$R(t) \quad = \quad R_0 + x(t), \tag{2}$$

where R_0 is the nomial position, and

$$x(t) \quad = \quad m\sin(\omega_m t) \tag{3}$$

is the vibration movement of the target with amplitude m and frequency ω_m. The round trip delay of the radar signal bouncing off the target is given by

$$t_d \quad = \quad \frac{2R(t)}{c} \; = \; \frac{2[R_0 + x(t)]}{c}, \tag{4}$$

which results in the following received signal.

$$r(t) \quad = \quad A\exp\left[j(2\pi f_c(t-t_d) + \pi K(t-t_d)^2)\right], \tag{5}$$

where A accounts for the amplitude change of the signal caused by the round trip propagation and reflection. For each chip, only the time period between t_d and T_r is used for mixing since the time period between 0 and t_d generates a high frequency signal that is usually filtered out. Within the valid period, the beat signal for a single chirp after mixing becomes

$$\begin{aligned} y(t) \quad &= \quad s^*(t)r(t) \\ &\approx \quad A\exp\left\{j\left[2\pi K t_d t + 2\pi f_c t_d\right]\right\}, \end{aligned} \tag{6}$$

where the term associated with t_d^2 is omitted because $t_d^2 << t_d t$. From (6), we can see that the round trip delay is directly related to the beat frequency and phase. However, the variation of $x(t)$ is very small within a single chirp. To obtain vibration signatures, we need to track the phase change of the beat signal across a sequence of L chirps. The round trip delay for the l-th chirp within the chirp sequence is

$$t_d \quad = \quad \frac{2[R_0 + x(lT_r + t)]}{c}. \tag{7}$$

Close inspection of $x(lT_r + t)$ generates the following approximation, considering that $\omega_m t$ term is small.

$$\begin{aligned} & x(lT_r + t) \\ = \quad & m\sin[\omega_m(lT_r + t)] \\ = \quad & m\left\{\sin(\omega_m lT_r)\cos(\omega_m t) + \cos(\omega_m lT_r)\sin(\omega_m t)\right\} \\ \approx \quad & m\sin(\omega_m lT_r). \end{aligned} \tag{8}$$

Except for t_d, the beat signal for the l-th chirp still has the same expression as in (6) because of the periodicity of the chirp sequence, i.e., $s(lT_r + t) = s(t)$, and $r(lT_r + t) = r(t)$. Therefore, we can substitute (7) and (8) into (6) and obtain

$$\begin{aligned} y(lT_r + t) \; = \; A\exp\Bigg\{j\Bigg[&\frac{4\pi K R_0}{c}t + \frac{4\pi f_c R_0}{c} \\ &+ \left(\frac{4\pi K t}{c} + \frac{4\pi f_c}{c}\right) m\sin(\omega_m lT_r)\Bigg]\Bigg\} \end{aligned} \tag{9}$$

After sampling and omitting $\frac{4\pi K t}{c}$ ($Kt << f_c$ in typical FMCW radars for $0 < t < T_r$), we have

$$y(lT_r + nT_s) \quad = \quad A\exp\left[j\left(\omega_b n T_s + \psi_l\right)\right], \tag{10}$$

where T_s is the sampling period and

$$\omega_b \quad = \quad \frac{4\pi K R_0}{c} \tag{11}$$

$$\psi_l \quad = \quad \frac{4\pi f_c R_0 + 4\pi f_c m\sin(\omega_m lT_r)}{c}. \tag{12}$$

In FMCW radar terms, the beat signal is a 2-dimentional function of the fast time n and slow time lT_r. The goal of the estimation algorithm is to find the vibration amplitude and frequency. In order to do that, we have to find estimates for ω_b and ψ_l from the sampled beat signal. Those can be obtained by running fast Fourier transform (FFT) on the fast time, usually referred to as the range FFT [9]. To illustrate the process, we take a N-point discrete-time Fourier transform (DTFT) on the beat signal, i.e.,

$$\begin{aligned} Y(e^{j\omega}, l) \quad &= \quad \sum_{n=0}^{N-1} \exp[j(\omega_b n T_s + \psi_l)]\exp(-j\omega n) \\ &= \quad \exp(j\psi_l)\exp[-(\omega - \omega_b T_s)(N-1)/2] \\ &\quad \times \frac{\sin\left[(\omega - \omega_b T_s)N/2\right]}{\sin\left[(\omega - \omega_b T_s)/2\right]} \end{aligned} \tag{13}$$

If we select $\hat{\omega} = \omega_b T_s$, i.e., the frequency corresponding the the maximum of DTFT output, then the DTFT output at that frequency only has the phase term, $e^{j\psi_l}$. In reality, FFT has limited resolution, the residue phase caused by imperfect frequency estimation can have an impact on the estimation of ψ_l term. Interestingly, if the DTFT is taken using index from $-N/2$ to $N/2 - 1$ in (13), then the effect of the residue term is much smaller since the DTFT introduces much less phase shift for $\hat{\omega}$ that deviates from the true $\omega_b T_s$.

4. CRAMER-RAO LOWER BOUND

In this section, we establish the CRLBs of vibration parameter estimation. The parameter estimation problem in (10) can be simplified into the estimation of the parameters of the following model given a block of N by L samples of $y(n, l)$.

$$\begin{aligned} y(n,l) \quad &= \quad A_1\exp\left\{j\left[\omega_1 n + \phi_1 + A_2\sin(\omega_2 l + \phi_2)\right]\right\} \\ &\quad + w(n,l), \end{aligned} \tag{14}$$

where $w(n,l)$ is assumed to be i.i.d. random variables following the complex Gaussian distribution with variance $2\sigma^2$. All model parameters, A_1, ω_1, ϕ_1, A_2, ω_2, and ϕ_2 are assumed to be real. To derive the bounds, we start with the probablity density function (PDF) of the noise, which is

$$p\left[w(n,l)\right] = \frac{1}{2\pi\sigma^2}\exp\left\{-\frac{1}{2\sigma^2}||w(n,l)||^2\right\} \quad (15)$$

Thus, the PDF of a block of $N \times L$ measured data given a set of model parameters is

$$p\left[\mathbf{Y};\boldsymbol{\theta}\right] = \prod_{l=0}^{L-1}\prod_{n=0}^{N-1}\frac{1}{2\pi\sigma^2}\exp\left\{-\frac{1}{2\sigma^2}||y(n,l)-A_1e^{j\alpha}||^2\right\} \quad (16)$$

where α is used to denote $\omega_1 n+\phi_1+A_2\sin(\omega_2 l+\phi_2)$ and $\boldsymbol{\theta} = [A_1,\ \omega_1,\ \phi_1,\ A_2,\ \omega_2,\ \phi_2]$. With the PDF function in (16), we can derive the Fisher information matrix for $\boldsymbol{\theta}$, which is given in (22). Note that in the Fisher information matrix, the terms that involve linear summation of sinusoidal functions of ω_1 and ω_2 are approximated by zero, which is valid for large N and L. The CRLBs of the estimators of the model parameters can now be found by examining the diagonal values of the inverse of the Fisher information matrix, which are

$$\mathrm{var}(A_1) = \frac{\sigma^2}{NL} \quad (17)$$

$$\mathrm{var}(\omega_1) = \frac{12\sigma^2}{A_1^2NL(N^2-1)} \quad (18)$$

$$\mathrm{var}(\phi_1) = \frac{2\sigma^2(2N-1)}{A_1^2NL(N+1)} \quad (19)$$

$$\mathrm{var}(A_2) = \frac{2\sigma^2}{A_1^2NL} \quad (20)$$

$$\mathrm{var}(\omega_2) = \frac{24\sigma^2}{A_1^2A_2^2NL(L^2-1)} \quad (21)$$

$$\mathrm{var}(\phi_2) = \frac{4\sigma^2(2L-1)}{A_1^2A_2^2NL(L+1)} \quad (23)$$

The variance for A_1, ω_1, and ϕ_1 are the same as those shown in [6] by using NL as the data length and setting the n_0 parameter in [6] to zero. The additional unknown parameters, A_2, ω_2, and ϕ_2 do not affect the bounds of those parameters. They are essentially decoupled except that the amplitude A_1 affects estimation accuracy of A_2, f_2, and ϕ_2.

To express the bounds directly in terms of FMCW parameters, we can utilize the following relationships obtained by comparing (14) and (10).

$$\mathrm{SNR} = \frac{A_1^2}{2\sigma^2},\ \omega_2 = 2\pi f_m T_r,\ A_2 = \frac{4\pi f_c m}{c}. \quad (24)$$

After substituting (24) into (20) and (21), the CRLBs for vibration frequency and amplitude are given by

$$\mathrm{var}(m) \geq \frac{c^2}{16\pi^2\ N\ L\ f_c^2\ \mathrm{SNR}} \quad (25)$$

$$\mathrm{var}(f_m) \geq \frac{3c^2}{16\pi^4\ T_r^2\ m^2\ N\ L\ (L^2-1) f_c^2\ \mathrm{SNR}} \quad (26)$$

As an example, for a typical set of FMCW parameters used in the automotive applications, i.e., $\mathrm{SNR} = 10$dB, $f_c = 76$GHz, $N = 875$, $L = 1000$, the standard deviation bound of the amplitude is 0.11 um. For a vibration amplitude of 10 um, the standard deviation bound of the vibration frequency is 0.04 Hz. From these numbers, we can see that the FMCW radar approach is capable of providing very accurate estimates of the parameters of a vibration signal.

5. PARAMETER ESTIMATION ALGORITHM

In this section, we set up simulations to verify the CRLBs presented in Section 4. The received data in the simulations were generated according to the signal model in (14) with the following parameters. A total of 500 random runs were performed to obtain variance of estimated parameters.

- $N = 128$, $L = 128$, $A_1 = 1$, $A_2 = 0.5$
- f_1 and f_2 uniformly distributed from 0.05 to 0.45
- ϕ_1 and ϕ_2 uniformly distributed from $-\pi/2$ to $\pi/2$

Parameter estimation is done in two steps. In the first step, for each l, we run FFT on index n and determine the frequency and phase corresponding to the maximum FFT amplitude, recorded as $\hat{f}_1(l)$ and $\hat{\phi}_1(l)$, respectively. The estimates for each l are then averaged across all chirps to generate the final estimates, $\hat{f}_1$ and $\hat{\phi}_1$. The simulation results for different

$$\mathbf{I}(\boldsymbol{\theta}) = \begin{bmatrix} \frac{NL}{\sigma^2} & 0 & 0 & 0 & 0 & 0 \\ 0 & \frac{A_1^2NL(N-1)(2N-1)}{6\sigma^2} & \frac{A_1^2NL(N-1)}{2\sigma^2} & 0 & 0 & 0 \\ 0 & \frac{A_1^2NL(N-1)}{2\sigma^2} & \frac{A_1^2NL}{\sigma^2} & 0 & 0 & 0 \\ 0 & 0 & 0 & \frac{A_1^2NL}{2\sigma^2} & 0 & 0 \\ 0 & 0 & 0 & 0 & \frac{A_1^2A_2^2NL(L-1)(2L-1)}{12\sigma^2} & \frac{A_1^2A_2^2NL(L-1)}{4\sigma^2} \\ 0 & 0 & 0 & 0 & \frac{A_1^2A_2^2NL(L-1)}{4\sigma^2} & \frac{A_1^2A_2^2NL}{2\sigma^2} \end{bmatrix} \quad (22)$$

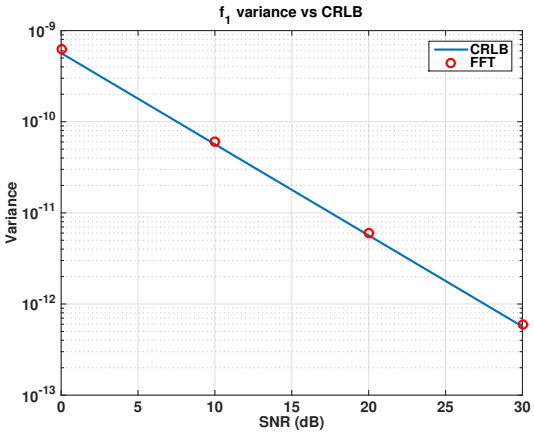

Fig. 3. Comparison between variances obtained in simulations and the CRLB for f_1.

SNRs are shown in Fig. 3. The results match well with the theoretical bounds.

In the second step, we estimate parameters f_2 and ϕ_2. A simple approach for achieving this is to unwrap the phase, $\hat{\phi}_1(l)$, recorded in the first step, remove its mean, and run another FFT on the resulting sequence. Then the frequency and phase associated with the maximum FFT output become the estimates of f_2 and ϕ_2. However, as shown in red circle markers in Fig. 4, the variances of the estimates obtained using this approach are significantly higher than the CRLB bounds.

The difference is caused by two main factors. The first one is the demodulation of $\hat{f}_1$. When we obtain $\hat{\phi}_1(l)$, we essentially demodulate each chirp by $\hat{f}_1(l)$ through the FFT process and then find the resulting phase. Although we have a more accurate estimate of $\hat{f}_1$, which is obtained through averaging $\hat{f}_1(l)$, it is not used in the process of estimating $\hat{\phi}_1(l)$. This inaccuracy causes larger variances in estimating f_2 and ϕ_2. A more accurate approach to obtain $\hat{\phi}_1(l)$ is

$$\hat{\phi}_1(l) \quad = \quad \frac{1}{N}\sum_{n=0}^{N-1} \angle\left[y(n,l)\exp(-j2\pi\hat{f}_1 n)\right] \qquad (27)$$

The second factor is the residue correlation in the basis functions of the FFT. This is not problem in f_1 estimation since f_1 is a complex tone, in which case the maximum likelihood (ML) solution does not rely on perfect orthogonality [6]. The vibration signal here is a real sinusoidal function. An accurate parameter estimation requires perfect orthogonality [10, p. 193] between the cosine and sine basis functions used in the FFT process, which is not possible for limited number of samples. To be more accurate, a least-square based grid search algorithm [10, p. 193] is required at the expense of significantly more computation than FFT. With more accurate frequency demodulation and least-squares, we can achieve variance close to the CRLB as shown in the green diamond markers in Fig. 4 for both f_2 and ϕ_2. Another source of errors in the variance of ϕ_2 using FFT comes from phase wrapping

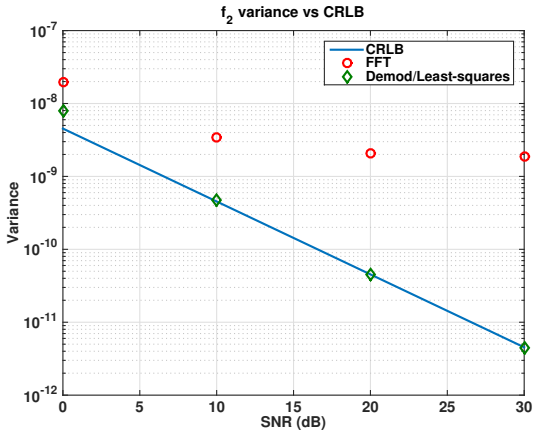

(a) Variance vs. CRLB for f_2

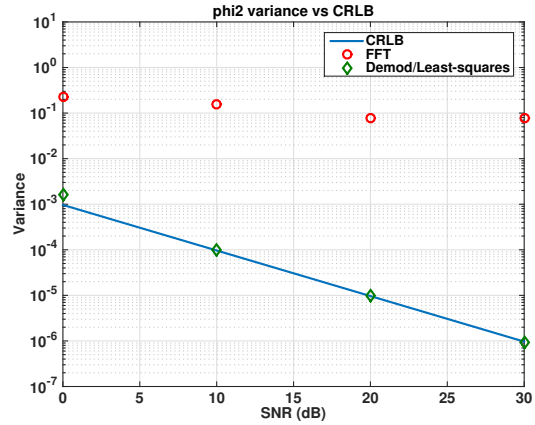

(b) Variance vs. CRLB for ϕ_2

Fig. 4. Comparison between variances obtained in simulations and the CRLBs for f_2 and ϕ_2.

around for a few inaccurate phase estimates, which causes very large errors. With the new estimation approach, this issue no longer affects results.

The two step approach presented in this section can also be shown to be the ML solution to the estimation problem in (13) by noticing the decoupling of the tone parameters in (22) and using arguments similar to those used in [6] and [10].

6. CONCLUSIONS

This paper presents detailed analysis on using FMCW radar for vibration parameter estimation. New CRLBs are established to understand the theoretical accuracy that can be achieved by the FMCW radar approach. The CRLBs are verified in simulations and can be achieved by the estimation algorithm developed in this paper. The analysis in this paper shows that vibration parameters measured with FMCW radar can achieve very good accuracy, which have the great potential to be used as precision non-contact vibrations sensors.

7. REFERENCES

[1] K. G. McConnell and P. S. Varoto, *Vibration testing: theory and practice*, John Wiley & Sons, Hoboken, N.J, 2nd edition, 2008.

[2] J. A. Rice, C. Li, C. Gu, and J. C. Hernandez, "A wireless multifunctional radar-based displacement sensor for structural health monitoring," in *Proc. SPIE, Sensors Smart Structures Technol. Civil, Mech. and Aerosp. Syst.*, Apr. 2011, vol. 7981.

[3] C. Li, V. M. Lubecke, O. Boric-Lubecke, and J. Lin, "A review on recent advances in Doppler radar sensors for noncontact healthcare monitoring," *IEEE Trans. Microw. Theory Techn.*, vol. 61, no. 5, pp. 2046–2060, May 2013.

[4] B. P. Ginsburg, S. M. Ramaswamy, V. Rentala, E. Seok, S. Sankaran, and B. Haroun, "A 160 GHz pulsed radar transceiver in 65 nm CMOS," *IEEE J. Solid-State Circuits*, vol. 49, no. 4, pp. 984–995, Apr. 2014.

[5] T.-Y. J. Kao, A. Y.-K. Chen, Y. Yan, T.-M. Shen, and J. Lin, "A flip-chip-packaged and fully integrated 60 GHz CMOS micro-radar sensor for heartbeat and mechanical vibration detections," in *Proc. IEEE Radio Freq. Integr. Circuits Symp.*, June 2012, pp. 443–446.

[6] D. Rife and R. R. Boorstyn, "Single tone parameter estimation from discrete-time observations," *IEEE Trans. Inf. Theory*, vol. 20, no. 5, pp. 591–598, Sept. 1974.

[7] G. Wang, J.-M. Munoz-Ferreras, C. Gu, C. Li, and R. Gomez-Garcia, "Application of linear-frequency-modulated continuous-wave (LFMCW) radars for tracking of vital signs," *IEEE Trans. on Microw. Theory Techn.*, vol. 62, no. 6, pp. 1387–1399, June 2014.

[8] P. Setlur, M. Amin, and F. Ahmad, "Cramer-Rao bounds for range and motion parameter estimations using dual frequency radars," in *Proc. IEEE Int. Conf. Acoust. Speech Signal Process.*, Apr. 2007, vol. 3, pp. III–813–III–816.

[9] D. E. Barrick, "FM/CW radar signals and digital processing," Tech. Rep. ERL 283-WPL 26, NOAA, July 1973.

[10] S. M. Kay, *Fundamentals of statistical signal processing*, Prentice Hall signal processing series. Prentice-Hall PTR, Englewood Cliffs, N.J, 1993.